CHAPTER 2

Preparation and Optical Properties of II-VI Semiconductor Nano-cluster and Polymeric Electro-optic Films

---

2.1 Introduction

2.1.1 General theories and concepts concerning semiconductor nano-crystals

Nano-materials or quantum dots/clusters have unusual properties in comparison with their bulk counterparts. Considerable theoretical and experimental efforts have been devoted in this field over the past 15 years, since they have potential uses in many areas, such as the electro-optics and nonlinear optics areas.

Quantum confinement and excitons are the main reasons for electro-optic and nonlinear optical phenomena. In nano-crystals, defect (hole) concentration at the interfaces is very high, and the average free path of electrons is very small. Outside the particle, the wave function is zero, corresponding to an infinitely large potential barrier, and the Coulomb interaction may be neglected [(1)]. So the bound electron-hole pairs and exciton concentration is very high. They can be excited to higher levels (excitation levels) near the conduction band by absorbing optical energy if the optical energy is larger than the exciton resonant energy. The excitons are not stable, and they may return to the

ground state and lose some energy by the interaction of excitons and phonons. The size contribution of nano-crystals to electro-optic and nonlinear optical effects is much larger than the intrinsic unit cell asymmetry contribution. So nano-crystals with symmetric unit cells (such as a cubic cell) still show electro-optic and nonlinear optical effects, but as the particle size becomes larger, surface defect and exciton concentrations decrease dramatically, bulk contribution becomes dominant, and electro-optic and nonlinear optical effects may disappear.

In order to understand the electro-optic and nonlinear optical effects, the general physical and chemical properties of nano-clusters is first reviewed here. The initial differences between bulk and quantum-confined low-dimensional substances are their different densities of states. Figure 2-1 depicts how the expected densities of states vary with dimensionality. Passing from 3-dimensions (3 D) to 2-dimensions (2 D) (quantum well) the density N(E) of states changes from a continuous dependence $N(E) \propto E^{1/2}$ to a step-like dependence. The steps correspond to allowed transitions between valence-band states and conduction-band states, while at each step, sharp peaks appear corresponding to confined electron-hole pair (exciton) states. For semimetals, as the crystal thickness L_x is reduced, both valence and conduction bands will break up into subbands, the bottom of the conduction band will rise up by an amount

$$\Delta E_e = \frac{h^2 \pi^2}{2 m_e^* L_x^2} \quad , \tag{2.1}$$

and the top of the valence band will drop by an amount

$$\Delta E_h = \frac{h^2 \pi^2}{2 m_h^* L_x^2} \quad , \tag{2.2}$$

where m_e^* and m_h^* are the electron and hole effective masses, and L_x is the crystal size.

The band overlap will decrease by $\Delta = \Delta E_e + \Delta E_h$, so the band gap increases, leading to metal-semiconductor-insulator transitions; the same effects occur for 1D and 0D systems.

With 0D (quantum boxes, dots, clusters, colloids, micro-crystallites, etc.) there are confinements in all three dimensions, and the energy levels for carriers change from continuous bands to a ladder of discrete levels. There is an enhanced volume-normalized oscillator strength of exciton features as the particle size R is reduced, due to the sharp electron-hole transitions in concentrated oscillator strength. In 0D systems, the primary energy terms are the electron-hole interaction energy, that is to say, the Coulomb term, and the confinement energy of the electron and hole.

To analyze the relationship between size and energy, suppose parabolic bands and infinite potential barriers at the surface of a spherical micro-crystallite. There are three cases for different relative particle sizes R in comparison with the exciton Bohr radius $(a_B)^{(2)}$, which is effective mass dependent and can be expressed as

$$a_B = a_e + a_h = 4\pi\varepsilon_0\varepsilon_r h^2/m_e e^2 + 4\pi\varepsilon_0\varepsilon_r h^2/m_h e^2 = 4\pi\varepsilon_0\varepsilon_r h^2/\mu e^2 \quad , \tag{2.3}$$

where $$\mu = m_h/(m_e + m_h) \quad , \tag{2.4}$$

a_e and a_h are the electron and hole exciton Bohr radii, respectively.

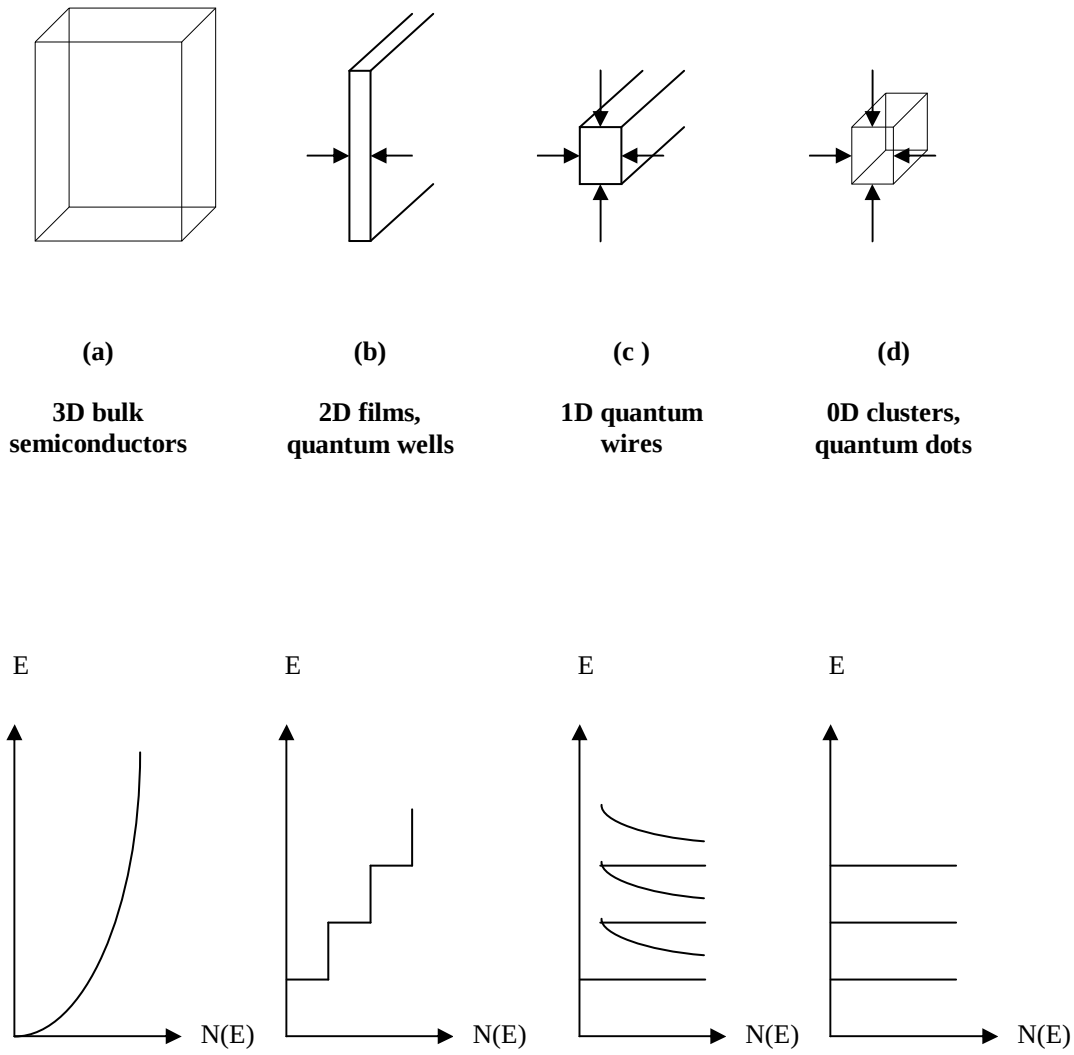

Fig. 2-1. Densities of states for 3D, 2D, 1D, and 0D systems.

There are three corresponding regions of the quantum confinement effect with respect to the particle size.

(A): Weak confinement ($R >> a_B$). Weak confinement of the exciton as a quasiparticle is preserved, there is a small increase in the exciton energy, and the features in the optical spectra move slightly to the blue (quantum blue shift).

(B): Medium confinement ($a_h < R < a_e$). Here the exciton binding energy is not very large and a_B can be very appreciable. The confinement effect is assumed to be important for the motion of the electrons, but the Coulomb force between electrons and holes is still important as it influences the motion of holes.

(C): Strong confinement ($R << a_B$). Both electrons and holes are quantized separately, and there is little spatial correction between them. The confinement energy is now the major term, and the Coulomb energy may be ignored.

Figure 2-2 illustrates the enhanced confinement and oscillation strength in compressed excitons. In bulk crystals, excitons have radius a_B , in quantum wells (2-D) and nano-clusters (3-D), the size of materials is comparable to or less than a_B , excitons are confined in a small region, enhanced electron and hole wave functions result, so the oscillation strengths of excitons are increased.

There are two major effects which are responsible for these size variations in nano-crystal properties due to changes in state density. First, the intrinsic properties of the interior of nano-crystals are transformed by the quantum size effect in nano-crystals. Second, the number of surface atoms is a large fraction of the total number of atoms.

Quantum size effect. As mentioned above, when the particle size is decreased to a certain value, electronic levels near the Fermi level (E_F) become discreet, and the

spacing (δ) between two adjacent levels varies with the number of electrons (N) in a system [3] by

$$\delta = \frac{4E_F}{3N} \propto V^{-1} \quad . \tag{2.5}$$

Thus, from Eq. (2.5), as the number of conduction electrons (N) in a system becomes infinite, the level spacing (δ) trends to zero. Instead, for nano-sized materials, δ

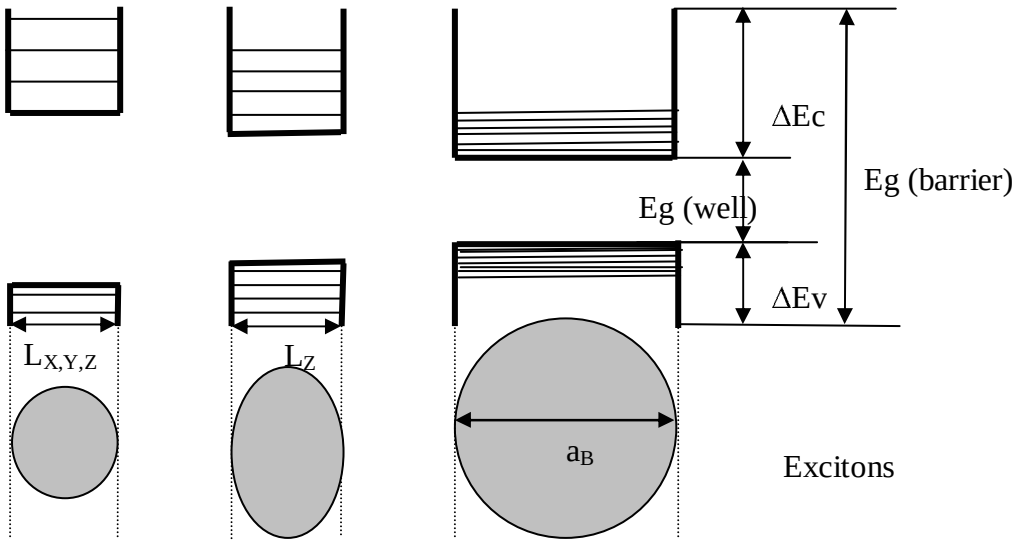

Fig. 2-2. Enhanced confinement and oscillation strength in compressed excitons.

Table 2.1: Number of total atoms and percentage of surface atoms vary with radius of nano-clusters.

Radius of nanocrystals(nm)	10	4	2	1
Number of total atoms	3×10^4	4×10^3	2.5×10^2	30
Percentage of surface atoms	20	40	80	99

may become comparable or even larger than the thermal, magnetic, electric and optical energies, and the quantum size effect must be considered. This effect may give rise to large differences of thermal, magnetic, optical, electrical properties between bulk and nano-sized materials. The critical size for quantum size effect can be determined by taking $\delta \geq kT$.

Surface effect. At the surface of a solid, the atomic bond structure comes to a sudden halt. As the radius of nano-crystals decreases for crystals of sizes indicated, the number of surface atoms increases rapidly, as is shown in Table 2-1.

Thus the surface energy of the nano-clusters also increases rapidly, and there are many unpassivated dangling orbitals. These are highly active, and easy to bond with other atoms. The periodic array of atoms in the surface region is disturbed, giving rise to changes in electron spin and energy spectra. In particular, the resulting dangling orbitals of unpassivated sites on the nano-crystal surface are highly polarizable, and the electron distribution around surface atoms is inherently highly noncentrosymmetric. This substantially contributes to a second-order nonlinear response [(4)]. The heavier hole has been predicted theoretically to have an enhanced probability of presence at the surface;

this leads to strong electron-hole charge separation in small nano-crystals. The corresponding presence of large dipole moments has been reported [5].

2.1.2 Synthesis of semiconductor nano-clusters

There are several methods now available to synthesize II-VI semiconductor nano-clusters. Several are based on classical nucleation-growth theory involving separation of the nucleation from the growth step. A fast nucleation first produces seed crystals that are almost identical. Then a slow growth period is followed, during which these seeds grow linearly with minimal broadening of the size distribution. For device figure of merit consideration, the generated particles should be pure, monodispersed (narrow size distribution), with high crystallinity, no or low defect concentration, high stability, and having robust surface passivation. The typical routes are as follows.

Colloidal routes. In this method, small particles are generated by the controlled precipitation of dilute colloidal solutions and the cessation of growth soon after nucleation. In order to produce nano-metric scale particles, nucleation and growth should be properly controlled. Small crystals, which are less stable, are redissolved and then recrystallized on larger and more stable crystals by a process which is known as Ostwald ripening. By employing this route, the quantum dots in question must have low solubility, which can be achieved by the correct choice of solvent, the pH, temperature and passivation agents. Highly monodispersed powders are obtained if the processes of nucleation and growth are distinctly separated, *i.e*, by fast nucleation and slow growth.

Synthesis in confined matrices. Materials which provide distinct defined cavities have been used to synthesis quantum dots. These well-defined zones have been used as

nano-metric sized reaction chambers. These matrix materials include zeolites, micelles, molecular sieves and polymers. The matrix can also determine the final properties of synthesized particles. For example, CdSe nano-particles can be produced in this way in inverse micell solutions. A microemulsion containing the metal ion is reacted with a silylchalogenide, resulting in nano-particles, and the surfaces capped by phenyl groups. Growing particles in the internal cavities of zeolites also limits the particle size of materials, to normally no larger than 20 nm. CdS nano-particles have been synthesized in two different zeolites by ion exchange from the sodium cationic form to cadmium cationic-form. Followed by exposure to H_2S gas, different sized particles were generated by varying the amount of cadmium used.

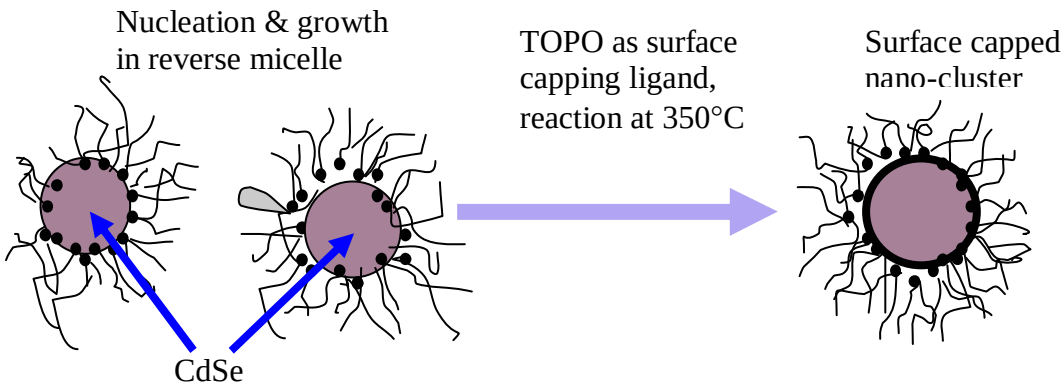

Fig. 2-3. Formation of surface capped semiconductor nano-crystals.

Metal-organic routes. In this method, a volatile metal alkyl (such as dimethylcadmium) and a chalcogen source is mixed in a solvent, then injected them into hot TOPO (tri-n-octylphosphineoxide). Nucleation is achieved by sudden introduction of the concentrated regents resulting in abrupt supersaturation and the formation of nuclei, followed by slower growth and annealing. The particles are passivated by a monolayer of the solvent ligands and hence can be isolated by solvents. Particles produced in this way are highly monodispersed and crystalline, and the particle size can be controlled by varying the reaction temperature. CdSe nano-particles prepared at 300°C having around one defect per nano-crystal have been achieved and quantum dots with fewer defects, formed by using higher temperature (350°C), have been reported [6,7,8] . Figure 2-3 illustrates the formation of surface capped semiconductor nano-crystals.

The growth of nano-particles can be achieved either in a glass matrix at elevated temperature (> 600 °C) or in a solution at much lower temperature (<350 °C). These two approaches are similar in theory, all related to nucleation theory, with the glass acting as an extremely viscous solvent. Glass and solution methods both have strong and weak points. For the solution method, we can control the surface of the crystallites and the generated particles can be extracted from the solution and treated as constituents in larger material systems. The surface of such particles can be modified by using different solvents and capping agents (ligands), so they can be made water soluble, and the ESA method (to be discussed later) can be used for thin film fabrication. As for the glass method, growth occurs at high temperature, and this should help achieve crystallinity and allow for the growth of larger particles than possible by the solution method.

Single molecule precursor route. Thermolysis of the air stable complex such as $[Cd(S_2CNEt_2)]_2$, it is safe, easy to handle, and high quality nano-clusters can be

synthesized. This process is very attractive because it is non-toxic, but the precursor is not commercially available and should be synthesized first.

Much progress in nano-clusters synthesis has been made now: high quality nano-clusters have been synthesized mainly by two research groups, one is Dr. C. B. Murray's group at the Department of Chemistry, MIT. Another is A. P. Alivisatos's group at the Department of Chemistry, University of Calfornia, Berkeley. They all used the metal-organic route, and the single molecule precursor route is also used recently, such as P. O. Brien's group at Department of Chemistry, Imperial College of Science, Technology and Medicine, UK. The key points for synthesis include: controlling reaction conditions such as temperature, time, pH value, concentration of solution, and using proper capping ligands (such as TOPO, PDDA), /solvent (such as pyridine, toluene), to isolate the particles. Some important facilities are needed, such as a fume hood, high speed centrifuge (higher than 4000 rpm) and temperature controller. Many analysis methods, such as UV-vis absorption spectra (UV-vis-abs), photo luminescence (PL), high resolution transmission electronic microscopy (HRTEM), atomic force microscopy (AFM), small angle neutron scattering(SANS), x-ray photoelectron spectroscopy(XPS), and X-ray diffraction can be used to characterize the synthesized clusters, to determine particle size, crystallity, surface state, band edge, and volume fraction. Also used are M-Z interferometers, to determine electro-optic properties.

2.2 Films Synthesis

2.2.1 Electro-static self-assembly (ESA) technique

Electrostatic self-assembly (ESA) is a type of thin film fabrication technique. It is based on the electrostatic interaction between anions and cations. Films are grown monolayer by monolayer, and each layer has a thickness of 1-10 nm. A wide variety of thin films with different properties can be made by this technique. Figures 2-4 and 2-5 illustrate the basic schematic of buildup ESA films. At first, the cleaned substrate is

charged by proper chemical processing, so negative surface charges are induced. This substrate is then dipped into a solution containing polyanions, and a monolayer is attached on the substrate by electrostatic attraction. Having been thoroughly rinsed by ion free ultra-pure water to remove any loose molecules, the substrate is then dipped into a polycationic solution to allow for the formation of another negatively charged monlayer. Subsequent polycation and polyanion monolayers are added in bilayer pairs by alternately dipping the substrate in polyanion and polycation solutions.

For electro-optic and nonlinear optic thin films made by the ESA technique, we may use electro-optic polymers or surface modified (charged) semiconductor nano-crystals (such as CdSe, CdS nano-particles) as polycations, or use other polymers such as poly(allylamine)hydrochloride(PAH) or polydiallyldimethylammonium chloride (PDDA) as polyanions, which have no electro-optic response. This process inherently produces noncentrosymmetric structures and large dipole moments, and such structure should give rise to large NLO and electro-optic responses. Because the internal electric field is produced by polycations and polyanions, and this helps to align the dipole moments of electro-optic polymers and semiconductor nano-crystals

The ESA technique has many advantages over traditional polymer electro-optic film processes [9, 10], such as spin coating, which is now most commonly used for waveguide layer fabrication. After electric field poling, spin coated EO polymer films usually degrade quickly, so that their EO coefficient decreases with time. In some cases, the EO response may finally disappear. On the other hand, in order to achieve high EO response, a high poling field (larger than 20V/micron) is needed, but for ESA-generated

EO films, no poling field is needed. Instead, the orientation of dipole moments or the noncentrosymmetric structure is retained via a strong internal electrostatic field. High

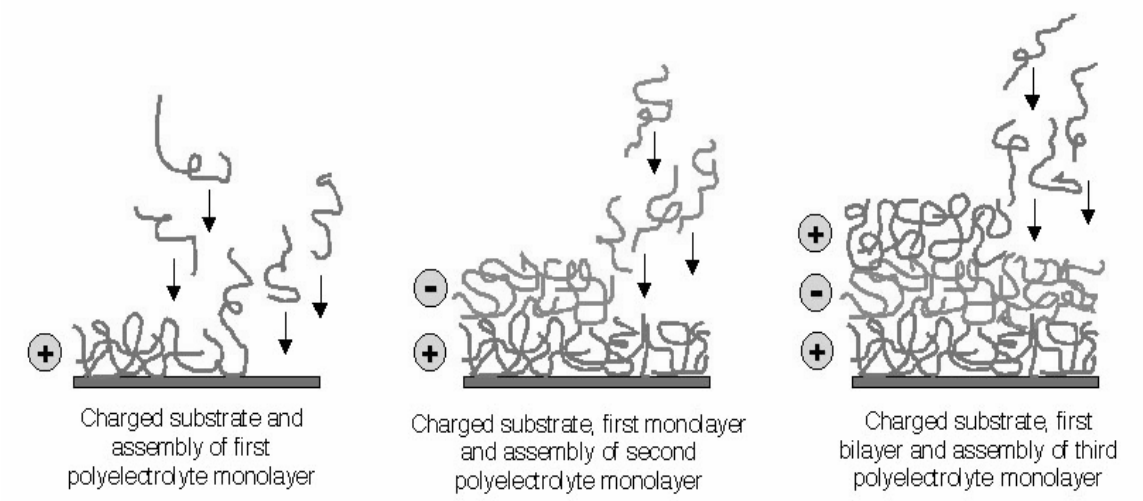

Fig. 2-4. ESA schematic for buildup of multilayer assemblies by consecutive adsorption of anionic and cationic molecule-based polyelectrolytes.

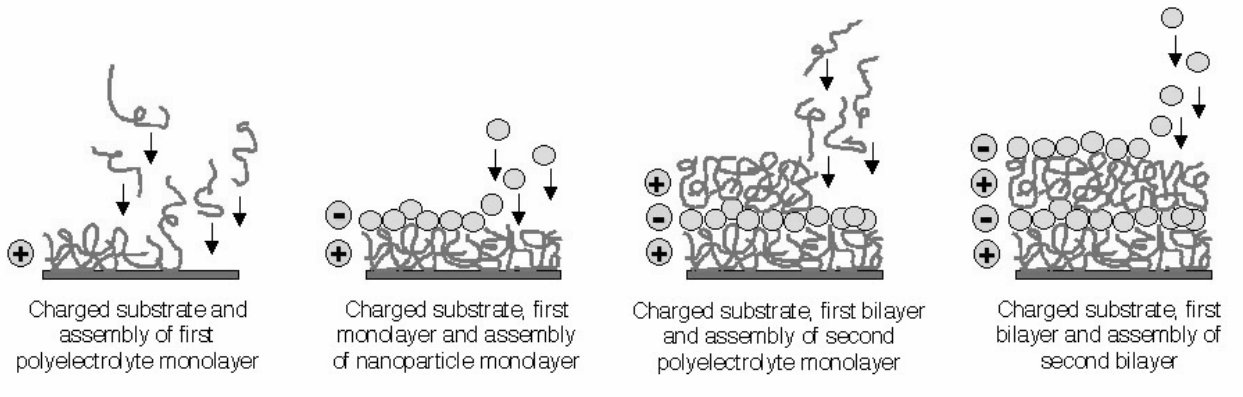

Fig. 2-5. ESA processing of polymers in combination with water-soluble nanocluster quantum dots allows wide variation of thin-film properties.

orientation of the EO polymer can be obtained, and high EO coefficient can be observed in the absence of external poling field, and, more importantly, it does not degrade with time. This is very useful for EO related device fabrication. ESA EO films are built up layer by layer, and each layer has thickness of the order 1-10 nm. The thickness of waveguide layers in integrated optic circuits is 1-10 microns, and device performances are closely related to the layer thickness, so stringent control of EO active layer thickness in device fabrication is important. In the spin coating processing, such thickness control on the order of a micron is difficult. In addition, ESA films are quite homogeneous leading to low waveguide scattering loss. The process is simple and highly repeatable, low cost, films are made under room temperature, and this processing is easily compatible with semiconductor VLSI technology. All of these advantages make EO film fabrication by the ESA technique very attractive. It is particularly suitable for integrated optical circuits.

2.2.2 Spin coating of nanoparticle doped polymeric EO films

Spin coating is a very popular film fabrication process. By the utilization of this technique, a solution or gel should be made first, composition of films can be easily controlled by changing the composition of solution or gel. Film thickness can also be easily controlled over wide range (nm-micron) by controlling the viscosity of solution or gel and the rotation speed of the spinner. The uniformity of spin coated films is higher than many other film processes, such as sputtering or evaporation and many (inorganic and organic) materials can be spun to form films.

2.2.3 Poling of spin coated electro-optic films

Spin coated electro-optic films must be poled in order to induce dipole moments and dipole orientation so as to result in electro-optic response. During poling, the temperature is raised close to the glass transition temperature. If the temperature is then lowered well below the transition temperature, the molecules are frozen into their new orientation. There are several kinds of poling processes, such as needle electrode corona poling, and parallel plate electrode poling. The former induces a circular poled region, the latter causes more uniform poling, but film damage may result, because of higher poling current, so in practice, the needle electrode corona poling configuration is more popular. In the case of a thin wire placed parallel to a planar electrode, the onset voltage of corona discharge occurs for[11]

$$V_c = (C_1 x + C_2 x^{1/2}) \ln(h/a) \quad , \qquad (2.6)$$

where x = pa/T, p is the air pressure, T is the temperature, a is the diameter of the wire, and h is the distance between the wire electrode and the plate electrode.

Once the corona discharge is initialized, the current produced between electrodes is

$$I_c = (V - V_c) V \mu C/p \quad , \qquad (2.7)$$

where V is the applied voltage, μ is the ion mobility, and C is a geometry dependent constant.

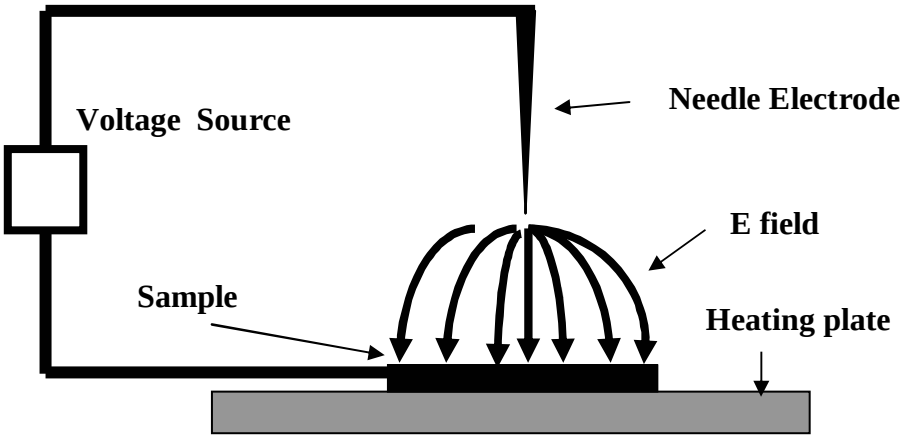

(a). Configuration

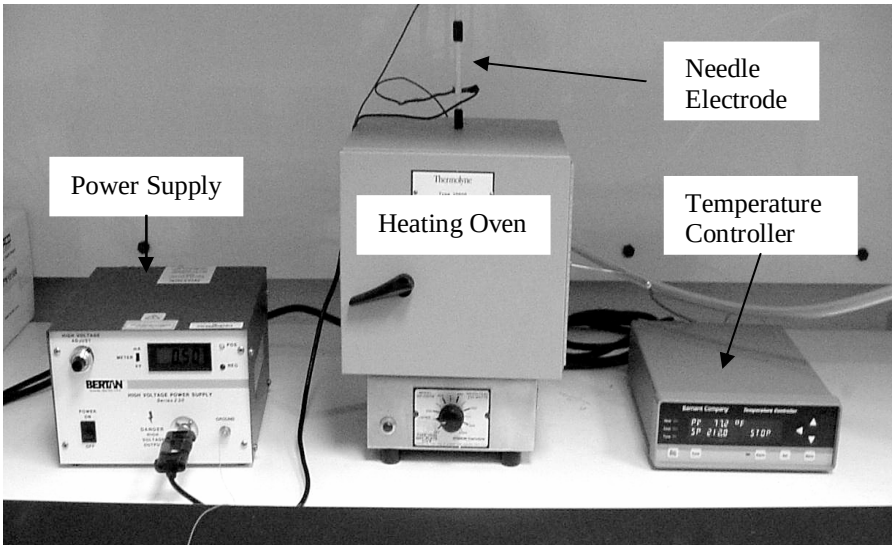

(b). Picture of poling set up

Fig. 2-6. Needle corona poling set up.

When the poling voltage is high, poling should be implemented in an inert atmosphere to avoid electric shorts. A needle corona poling set up is illustrated in Figure 2-6.

2.3 Characterization of fabricated nano-clusters and e-o films

Optical absorption (abs.) and photo luminescence (PL) of fabricated nano-clusters and electro-optic films were characterized by UV-vis absorption spectra (U-2001 Spectrophotometer, Hitachi Instrument Inc. scan speed 400nm/min and slit width 2 nm) and photo luminescence spectra(F-4500 Fluorescence Spectrophotometer, Hitachi Instrument Inc.) , FT-IR(FTS 6000 Spectrometer, Hitachi Instrument Inc.). Images were obtained by atomic force microscopy (AFM) (NanoScope, Digital Instrunments), using the tapping mode to image the surface morphology of films with atomic resolution. Images were also obtained using high resolution transmission electric microscope HRTEM **(**Philips-420 T electron microscope) operation at 100kV). HRTEM images were carried out in bright field. Cluster samples were prepared by first dispersing nano-clusters in toluene and then placing a drop of the dilute dispersion of nano-clusters on the surface of carbon coated copper grids. XPS spectra were used to detect the composition of samples, using an XPS spectrometer (Perkin-Elmer-5400), equipped with an X-ray Mg anode, and operated voltage of 14Kv. Data were obtained with Mg k_α radiation (1253.6eV) at a power of 300 W. Survey scans were collected over the range 0-1100 eV. Close-up scans were collected on the peaks of interest for the different elements with a 71.5 eV pass energy detection and a resolution of 1 eV. A base pressure of 10^{-8} Torr was

maintained during the measurement. Film thickness and optical index were measured using ellipsometers (Rudolph/Auto EL at fixed wavelength 632.8 nm and Woollam VB-200 at variable wavelength 200~1030 nm).

2.4 Experimental procedure

2.4.1 II-VI semiconductor nano-cluster and film preparation

CdS nano-clusters have been prepared by the high temperature solution method. Dimethyl cadmium [$Cd(CH_3)_2$] and bis(trimethylsilyl) sulfide [$(TMSi)_2S$] were dissolved in trioctyphosphine [$(CH_3(CH_2)_7)_3P$, TOP], in a nitrogen saturated dry box. They were

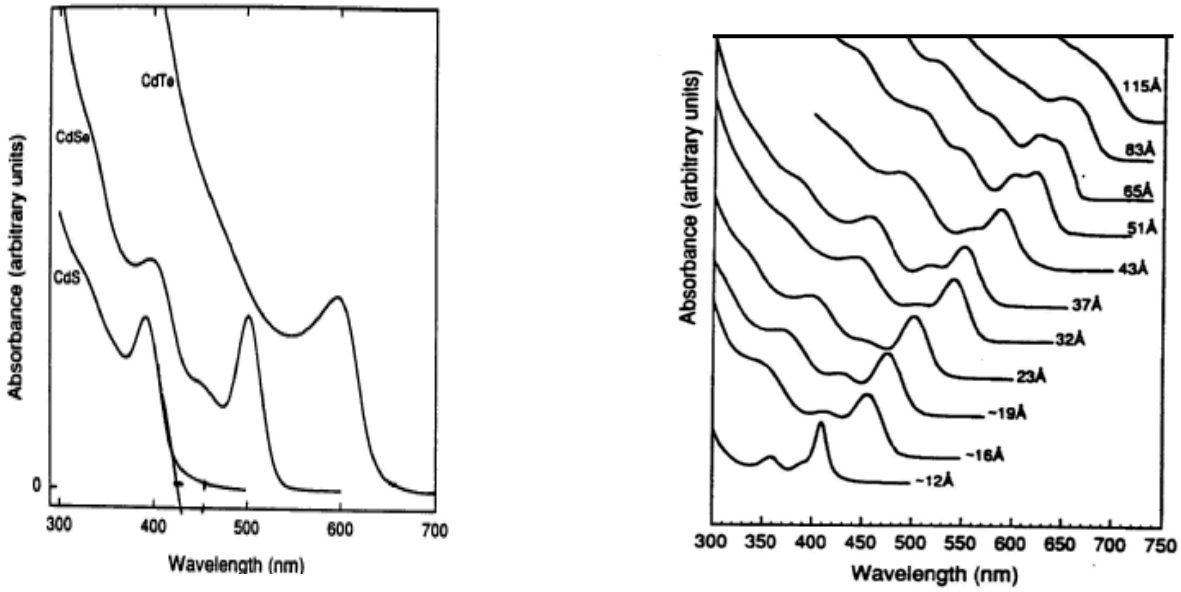

(a). 2-3 nm diameter of CdSe, CdS, and CdTe nano-particles

(b). CdSe nano-particles at various sizes

Fig. 2-7. Room temperature absorption spectra of CdS, CdSe and CdTe nano-crystallites with different particle sizes.

mixed together at room temperature, then injected into preheated trioctyphosphine oxide[$(CH_3(CH_2)_7)_3PO$, TOPO]. The cadmium and selemium organo-metallic precursors immediately deposited at high temperature (300--350°C) to form CdS as seeds, and the solvent TOPO served as a capping agent. It binds to the cadmium sites of the small CdS seeds by its oxygen atoms, with the octyl groups sticking out. This creates an effective barrier which remarkably reduces the reactivity of the particles, so the growth speed is slowed down. The reaction proceeds within several hours, the particle size increases with time, and the reaction was monitored by measuring the absorption spectrum or luminescence spectrum of reaction solution regularly. Different particle size corresponds to different peak positions of absorption and luminescence spectra. Approximate estimation of the particle size can be obtained simply by watching the color of the solution. Peak position and particle size of CdS and CdSe nano-particles in absorption spectra are illustrated in Figure 2-7 [12, 13].

2.4.2 Preparation of electro-optic films by ESA technique

CdSe quantum dots modified with mercaptoacetic acid were prepared by the addition of 30 mg of mercaptoacetic acid and 30 mg of CdSe quantum dots to 20 ml of methanol under nitrogen. The pH was adjusted to 10 by addition of tetramethylammonium hydroxide, and the reaction mixture was refluxed for 4 hrs. The mercaptoacetic acid-passivated CdSe quantum dots were purified by several cycles of precipitation with acetone followed by dissolution in methanol. Finally, the CdSe quantum dots were dissolved in pH 10 water at 2 mg/ml to form a solution for the formation of ESA films. Poly(diallyl dimethyl ammonium chloride) (PDDA) was

purchased from Aldrich. PDDA was diluted to 1% and contained 0.5M NaCl at a pH of 7.5. ITO coated glass was used as the substrate. Multilayer CdSe/PDDA films were assembled by following manner: the ITO-coated glass substrates were cleaned thoroughly using a solution of acetone and isopropyl alcohol, then rinsed extensively with ultrapure water. The cleaned substrate was first immersed in a cationic 1% PDDA (v/v) aqueous solution for 1 minute, then rinsed extensively in ultrapure water, forming a monolayer of PDDA molecules. Immersion in the anionic aqueous solution of CdSe nano-clusters for one minute, again followed by thorough rinsing in ultrapure water, produced a uniform CdSe cluster monolayer on the top film surface. Subsequent bilayers were added by repetition of this alternating two-step process, until the desired thickness was achieved.

Polymer films may also be prepared by the ESA process: A number of commercially available polymer dyes show EO response, such as poly S-119, polyR-478 and PCBS. They are available from Sigma-Aldrich, are polycationic and water soluble. Also PDDA and PAH can be used as polyanion, and the concentrations of these solutions are approximately 5×10^{-2}—10^{-3} M.

2.4.3 Spin coating of nano-particle doped polymeric EO films

Nano-particles were mixed with Norland optic glue with a concentration between 0.5 –5 %(vol.). The mixture was stirred by a magnet bar then further mixed by ultrasonic vibration for 2 hr. Films were fabricated on ITO coated glass, by spin coating. Film thickness was controlled within 5-100 microns by varying the spinning speed. Transparent ITO coatings served as electrodes for electro-optic response measurement. Films were cured by UV light at a wavelength of 365 nm for 5 min. This method is

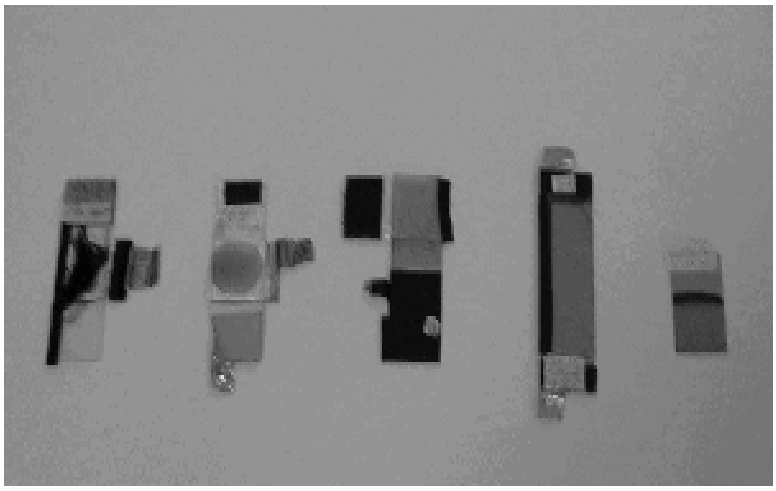

Fig. 2-8. Pictures of various films ready for measurements.

simple, and easy to control, in comparison with other methods, such as the dispersion nano-particles in epoxy and polymeric glass (PMMA). The films were subjected to poling at elevated temperature(>90°C) for 60 mins, where the poling voltage was 4 kV and the distance between electrodes was ~2cm. Figure 2-8 shows various films ready for measurements.

2.5 Results and discussion

2.5.1 Absorption spectrum and nano-cluster synthesis

In optical absorption of semiconductor quantum dots, absorption is related to the excitation of electrons from the ground state to the excited state, and the absorption coefficient decreases rapidly with the wavelength of the beams. For bulk semiconductors,

without the consideration of size effect, near the absorption edge, the absorption coefficient can be expressed as [14]

$$\alpha \sim (h\nu - E_g)^{\gamma} , \qquad (2.7)$$

where $h\nu$ is the photon energy, E_g is the bandgap, and γ is a constant.

Near the absorption edge, where $h\nu - E_g$ becomes comparable with the binding energy of a exciton, the Coulomb interaction between the free hole and electron must be taken into account. For $h\nu < E_g$, the absorption merges continuously into the absorption caused by the higher excited states of the exciton. When $h\nu >> E_g$, higher energy bands participate in the transition processes, and complicated band structures are reflected in the absorption coefficient.

On the other hand, optical absorption can be explained with respect to the exciton oscillator strength model. In bulk materials, the oscillator strength density is uniform over all K space, so the absorption coefficient is proportional to the density of states in K space and increases rapidly with energy above the band gap. As a result almost all of the oscillator strength exists above the gap in transitions creating free electrons and holes. In the case of excitons, because of the confinement effect in a small space, there are enhanced overlap of electron and hole wavefunctions. The more compact the exciton wave function, the higher the values of K space, and the greater the exciton oscillator strength, so the higher the optical absorption coefficient.

The nano-cluster synthesis process can be controlled by means of absorption and photo

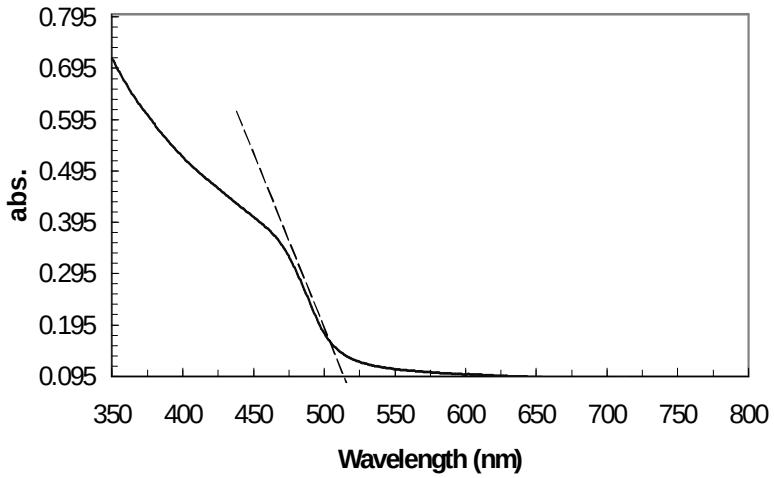

Fig. 2-9. Optical absorption spectrum of CdS anao-particles dispersed in pridine.

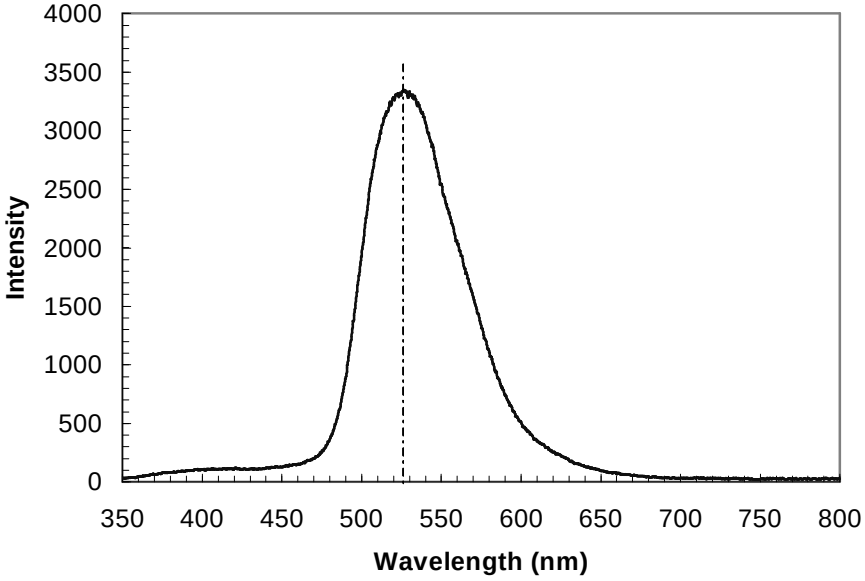

Fig. 2-10. Luminescence spectrum of CdS solution (CdS dispersed in pridine). Peak intensity is at 526.6 nm.

luminescence measurements. Two examples are demonstrated here; one is large CdS clusters, the other is small CdSe clusters. Figure 2-9 shows the room temperature absorption spectrum of CdS nano-particles synthesized in our laboratory. The threshold is about 508nm. Figure 2-10 shows the luminescence spectrum of the same sample, where the peak position is at 526.6 nm. Comparing this data with the band edge of bulk CdS (512 nm, 2.42eV), only a slight blue shift is observed, because the produced particles are still fairly large. The particle size can be reduced by decreasing the reaction time or temperature. The reaction and the absorption threshold of 2-3 nm diameter CdS is about 420 nm[(12)], and the exciton Bohr radius of CdS and CdSe are 3 nm and 5.4 nm respectively. CdS particles having this size have a threshold of about 425 nm. In order to achieve strong quantum confinement effects, CdS should have smaller size than CdSe; that is why CdSe nano-particles are more widely be used. But synthesizing CdSe particles is more difficult than CdS, because CdSe is extremely toxic and expensive facilities are needed. So better control of processing is needed obtain smaller, defect-free and impurity-free CdS particles.

In order to synthesize high quality quantum dots, it is important to choose proper precursors, ligands, solvent, control reaction temperature and time. Now the most widely used precursors are metal-organic compounds such as bis(trimethylsilyl)-sulfid [$(TMSi)_2$ S], bis(trimethylsilyl)selenium[$(TMSi)_2$ Se], and trioctylphosphine selenide[TOPSe] as S and Se sources, dimethylcadmium[Me_2Cd] as a Cd source. They are also used as precursors in MOCVD to deposit CdS(Se) films, because they are easy to thermolyze at moderate temperature, and they are stable and easy to prepare. The coordinating solvent

is critical in controlling the growth process, and stabilizating the resulting CdSe or CdS nanoclusters, and electrically passivating the particle surface. TOP/TOPO have been proved to be good both as solvent and capping groups, because their molten points are high, and match the nucleation and growth temperatures of CdSe and CdS nanoclusters. They also provide a controllable slow and stable growth environment for those nano-clusters, because they can attach to the Cd sites at the cluster surface, cap the clusters, present a significant steric barrier to the addition of material to the surface of a growing crystallite, thereby slowing the growth kinetics. Steady controlled growth results in highly monodisperse particles with consistent crystal structure. Many other solvents / capping species can not provide steady controlled growth. But these chemicals are in general very toxic, and not stable in air, so particle preparation must be made in a dry box and well vented fume hood. Recently researchers are seeking less toxic, air stable chemicals such as CdO as precursors [15], or using air stable single precursors to improve the process.

In order to modify the surface properties, TOP/TOPO can be replaced by other capping ligands right after the reaction. Many ligands are available, but the result obtained with different ligands are different. Ligands with more steric hindrance do not passivate the resulting nano-particle surface as well as less bulky groups. The solubility of particles changes with the surface chemistry. Capping ligands with longer hydro-carbon tails make the particle more soluble in organic solvents. This is helpful to keep the particle from precipitating, so the solution is more stable over time. By means of surface modification, properties of nano-particles can be altered. The photo luminescence spectrum changes very little, because there is no excitation transfer from the nano-

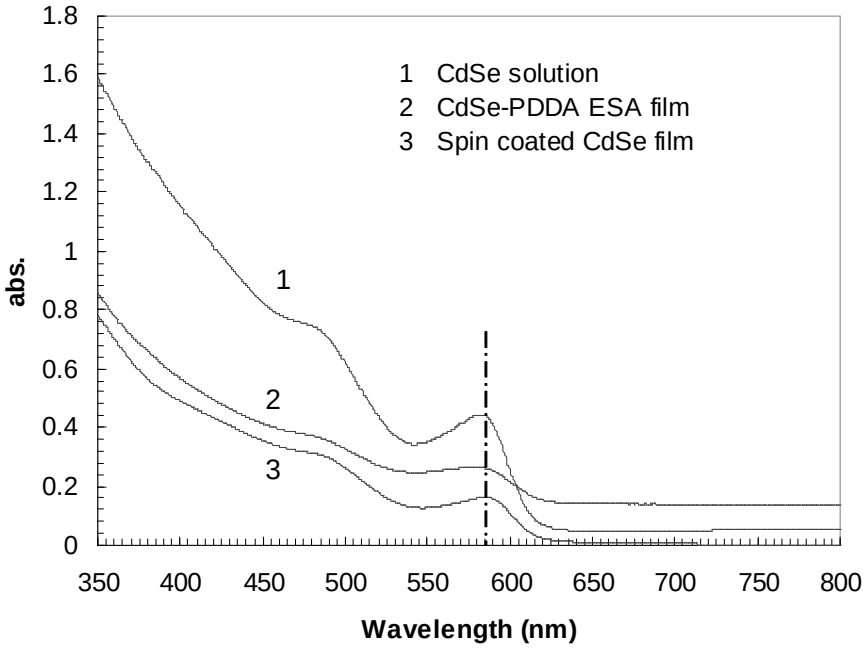

Fig. 2-11. Optical absorption spectra of CdSe films and solution.

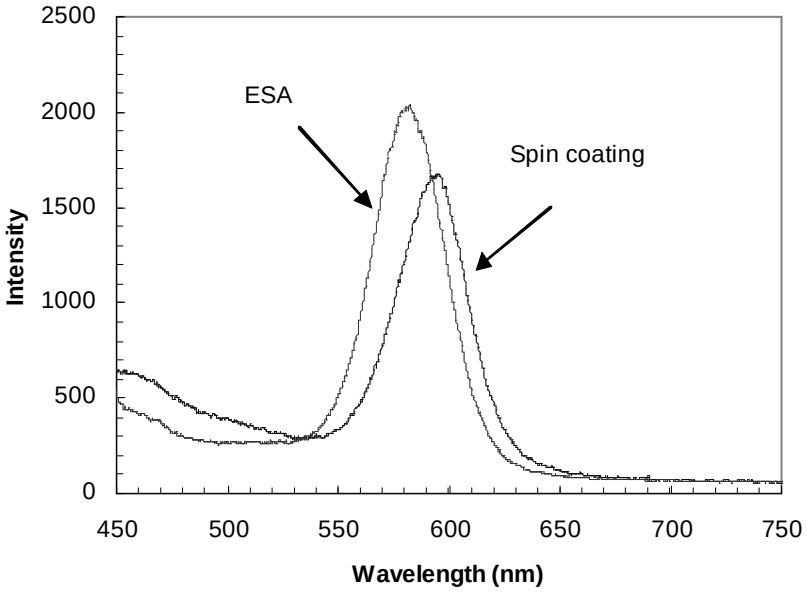

Fig. 2-12. Luminescence spectra of CdSe films fabricated by spin coating and ESA.

particles to the capping ligands. The absorption edge (so the band gap), and the absorption oscillator strength are unchanged by different surface chemistries, but better surface passivation and stronger bond strength enhance luminescence intensity, and the relaxation time of trap states is somewhat affected by surface chemistry.

In the case of CdSe nano-cluster synthesis, small nano-clusters are obtained. Figure 2-11 shows the absorption spectra of CdSe solution and films, it is noted that the band edge of the lowest 1S – 1S state is apparently shifted from the nominal value of 716 nm for bulk CdSe (at room temperature, at 15K, it is 680 nm) [(11)] to about 585 nm, so the particle size is 5-6 nm, which is small compared with its exciton Bohr radius. Strong quantum confinement is thus expected. From Figure 2-11, the absorption of a CdSe/PDDA film made by ESA processing is larger than that of a spin coated CdSe film, but the thickness of the spin coated film is 400 times thicker than that of ESA films. As a result the absorption coefficients of ESA films are much higher than those of spin coated films. This is one of the most important differences between spin coating and ESA processing for film fabrication. This is attributed to the related resulting molecular alignment and will be discussed in details below.

Figure 2-12 shows the luminescence spectra of two films. Their peak positions are quite close to those of absorption spectra, and there is a slight difference of peak position between the ESA and spin coated films. Mainly, two reasons contributed to these differences. First, the structure of ESA and spin coated films are different; this will be discussed below. Second, ESA films have a lower peak position and threshold, because the ESA film was made in a water solution, and size selection processing was done

automatically due to the precipitation of larger particles, and a better size distribution was reached.

Comparing the absorption and photo luminescence spectra in Figures 2-9, 2-10 and Figures 2-11, 2-12, there are some differences in peak positions of absorption and in the spectra. The differences are mainly due to defects or trap states. For ideal crystals without any defects, only two levels (the ground level and an excited level) exist and excitation and recombination occur only between these two levels, when the gap difference is Eg. In this situation, absorption and photo luminescence all correspond to a direct band transition with the same band gap Eg. But for our nano-clusters, many states may be created in between the valence band and the conduction band, such as surface states because of various surface defects, dangling bonds, and various traps (shallow, deep traps). They give rise to intraband transitions and affect the overall transition band gap slightly. Besides this, they have different lifetimes and decay rates upon excitation optically or electrically. Since absorption is effectively the reverse of photo luminescence, these states perform differently in optical absorption and photo luminescence. So different absorption and photo luminescence peaks result, and the amplitude of the difference is a measure of the quality of the produced particles, in that the greater the difference between the absorption and photo luminescence peaks, the larger the number of defects, and vice versa.

In order to compare the particle size results obtained from absorption spectra, transmission electronic microscopy (TEM) was implemented to obtain images of CdS and CdSe nano-clusters. Their images and diffraction patterns are showed in Figures 2-13 and 2-14.

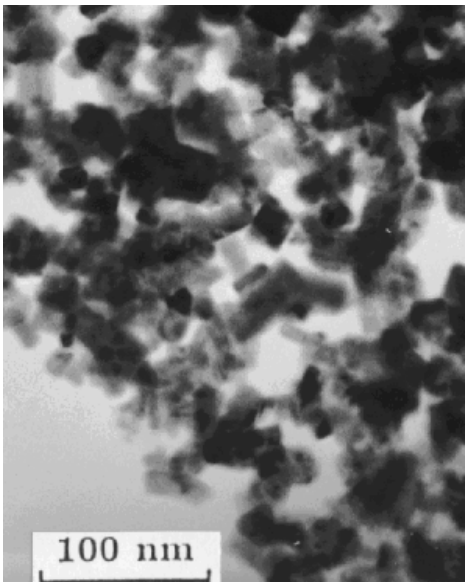

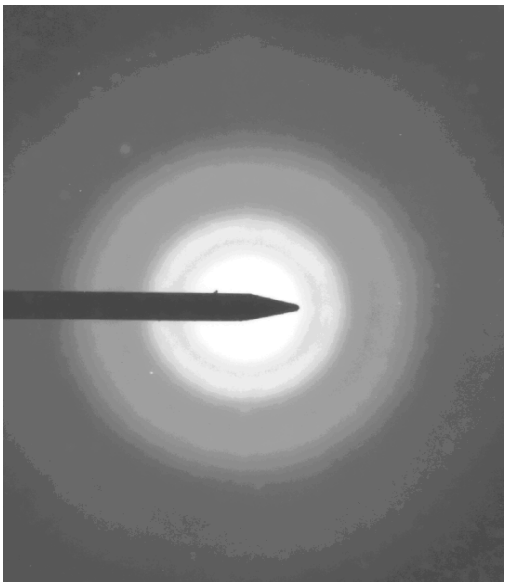

(a). TEM **(b). Diffraction ring**

Fig 2-13. TEM (A) and diffraction ring (B) of CdS nano-clusters.

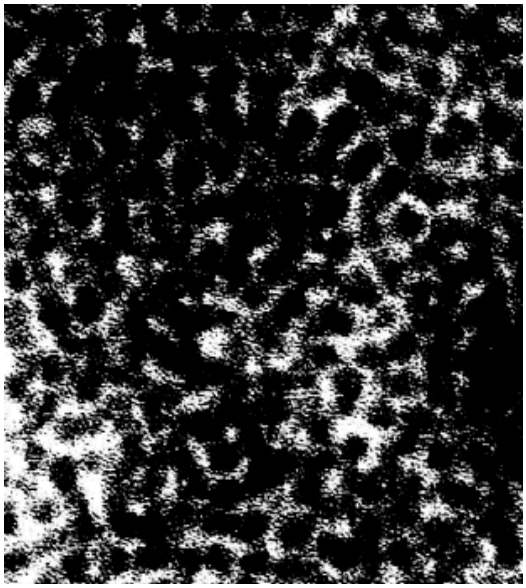

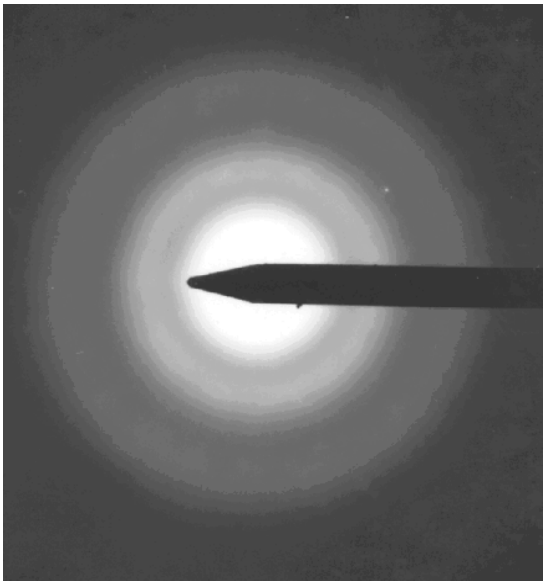

(a). TEM **(b). Diffraction ring**

Fig. 2-14. TEM (A) and diffraction ring (B) of CdSe nano-clusters.

From the TEM image of the CdSe particles, the particle size observed to be approximately is 4-6 nm, with narrow size distribution. This result is very similar to the particle size dataobtained from UV-vis absorption spectra by comparison with other group's results [8,16].

From the electronic diffraction pattern, there are no sharp diffraction rings. The broad diffuse rings observed are due to the small size of the crystallites. The patterns also show no spottiness. The breadth of the ring pattern depends upon the size and the number of crystals contributing to the pattern. This ring pattern indicates that the CdSe clusters are small and uniform. Clusters synthesized by this method normally possess a hexagonal structure (HCP). Here this is proven by the ratio of square of radius of 3 rings ($R_1^2 : R_2^2 : R_3^2$) = 1:3:9. But for very small particles, analysis of diffraction pattern rings is not appropriate, because the size of probe electronic beam is comparable to or even larger than the size of detected particles.

2.5.2 Analysis of the shifts of absorption spectra because of particle size

Particle sizes measured from absorption spectra and TEM images are very close. As demonstrated above, radium change of the nano-clusters leads to wavelength shift in absorption and luminescence spectra. This effect can be analyzed based on the Schrodinger's equation in quantum mechanical theory, where the exciton can be described by the Hamiltonian[17]

$$\hat{H} = -\frac{h^2}{2m_h}\nabla_h^2 - \frac{h^2}{2m_e}\nabla_e^2 - \frac{e^2}{\varepsilon|r_e - r_h|} \quad , \tag{2.8}$$

where m_h and m_e are the effective masses of holes and electrons, respectively, ε is the dielectric constant, and Hamiltonian, kinetic, Coulomb and polarization terms are include. The polarization term can be ignored because it is small in comparison with kinetic and Coulombic interactions. The wave function of excitons can be found, so the energy state of the excitons can be determined. With the wave function, the energy of the lowest excited states becomes

$$E(R) = E_g + \frac{h^2\pi^2}{2\mu R^2} - \frac{1.786e^2}{\varepsilon_2 R} - 0.248E_R \quad , \tag{2.9}$$

where

$$\frac{1}{\mu} = \frac{1}{m_e^*} + \frac{1}{m_h^*} \quad . \tag{2.10}$$

This equation also describes the effect that the band edge of the absorption spectrum varies with particle size. In equation 2-9, the first term is the bulk energy gap. The second term is the kinetic term, corresponding to quantum localization energy because of the quantum confinement effect, and proportional to $1/R^2$. The third term is the Coulombic term proportional to 1/R, and the last term is correlation energy. As the particle size is small, the kinetic term predominates. Based on this equation, the absorption band edge energy and wavelength shift varying with the particle size of CdS quantum dots are plotted in Figures 2-15 and 2-16.

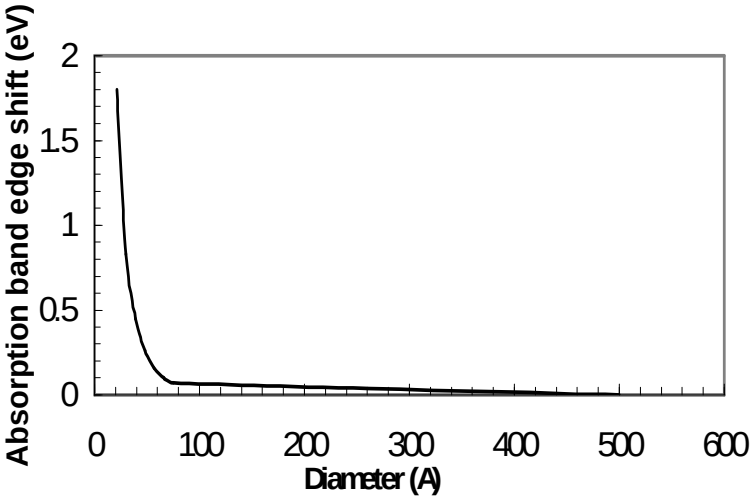

Fig. 2-15. Calculated absorption band edge varies with the diameter of CdS quantum dots.

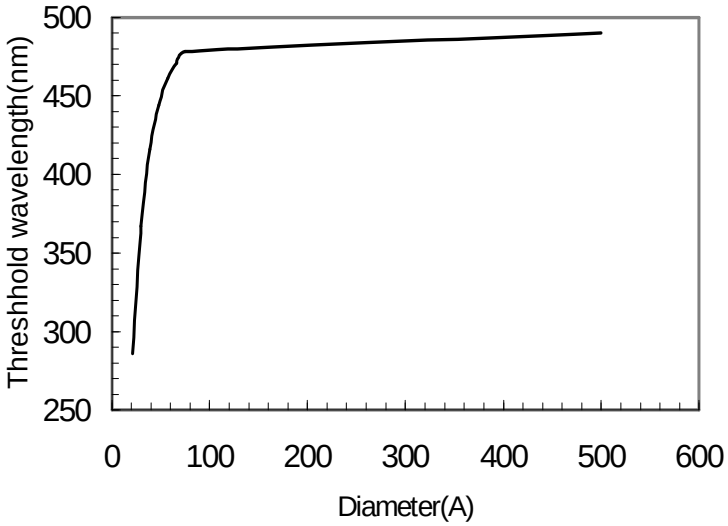

Fig. 2-16. Calculated threshold wavelength shift varies with the diameter of CdS quantum dots.

Comparing this calculation result with absorption and TEM measurement results, it can be found that at the same particle size, the actual shift is smaller than the calculated shift, since this model overestimates the shift for smaller clusters. The discrepancy means that this is a simple model, and that more factors should be considered.

2.5.3. Internal field of films induced by ESA process

Another kind of shift in optical absorption is due to the electro-optic Stark effect. This effect is also based on the quantum mechanical theory of wave functions, and the analysis of several kinds of interaction, as discussed above. But the shift in optical absorption originates from another factor, namely, the external or internal electrical field of samples.

In the analysis, the simplified model ignores the Coulomb interaction, and the anisotropic parts of the whole Hamiltonian. As the field F is applied, some oscillator strength is redistributed into transitions that are blocked for the non-field case. The second order perturbation theory may then be applied, leading to the shift [18]

$$\Delta E(F) = \frac{-0.65(eFR)^2}{E_{1s}} \quad , \tag{2.11}$$

where

$$E_{1s} = \frac{h^2\pi^2}{2R^2}\left(\frac{1}{m_e} + \frac{1}{m_h}\right) \quad , \tag{2.12}$$

R is the radius of the particles. From the theory, the shift ΔE is proportional to R^4 and F^2. F can be either an external applied field, or an internal field. For the molecular or

polymer Stark effect, F is an internal field, which can be caused by a number of factors, such as the ESA process, or film fabrication under the effect of an external field (field assisted ESA).

Within this model of the effect, another result is the change of optical density (OD) in the presence of an external or internal electrical field. This can be expressed as

$$\Delta OD(\omega) = \frac{C_x}{30\hbar^2} F_{\text{int}}^2 \frac{d^2(OD)}{d\omega^2} \quad , \tag{2.13}$$

where h is Planck's constant, F_{int} is the strength of the field inside the clusters and C_x is a scaling factor, related to the change in the dipole moment[19]

$$C_x = 5\Delta\mu^2 + 2\Delta\mu^2 (3\cos^2 \alpha - 1) , \tag{2.14}$$

where α is the angle between the field and the polarization vector of the light, and $\Delta\mu$ is the change in the dipole moment. This model is applicable for quantum dots and conjugated molecular or chromophores.

Figures 2-17, 2-18 and 2-19 show the peak position, optical density (OD) and wavelength at maximum absorption of PS-119/PDDA films. Two kinds of samples were fabricated and measured: one was made without an external field, the other one was made in the presence of a 0.47 volt potential during ESA process. The distance between the film substrate and the electrode was 5mm. The other conditions are the same between the two samples. The two samples were made using the same PS-119 and PDDA solutions. ITO coated glass substrates were cleaned in the same batch, and the optical absorption

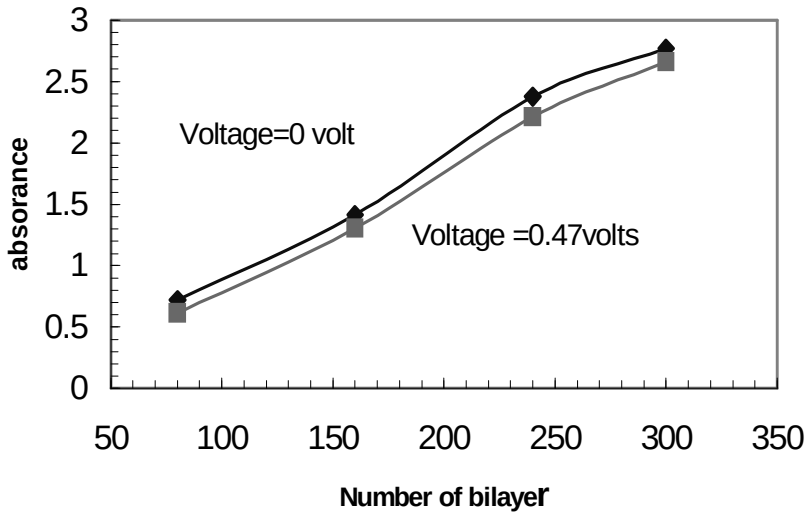

Fig. 2-17. Maximum absorption varies with thickness (number of layers) and external voltage of PS-119/PDDA films with and without external electrical field.

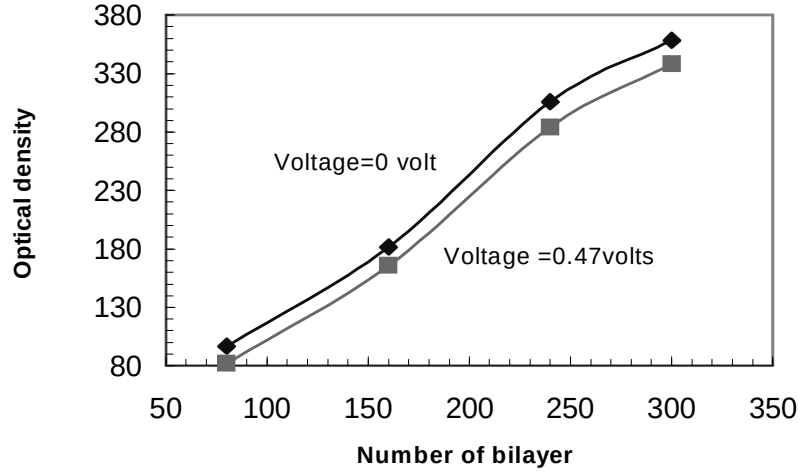

Fig. 2-18. Optical density varies with thickness (number of layers) and external voltage of PS-119/PDDA films with and without external electrical field.

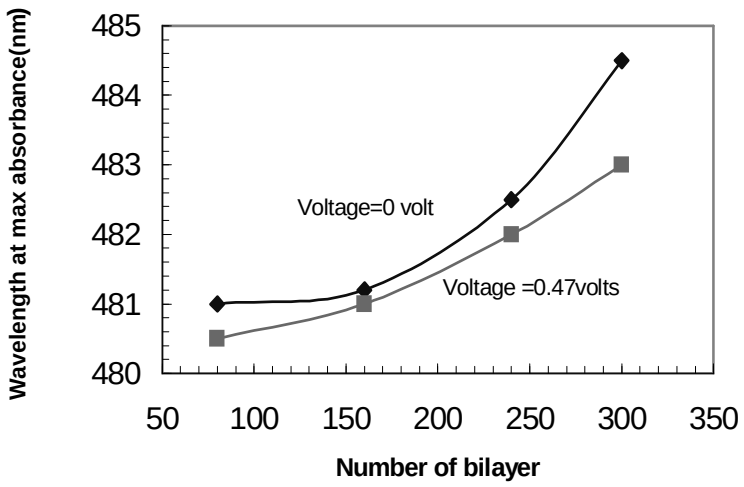

Fig. 2-19. Peak wavelength varies with thickness (number of layers) and external voltage of PS-119/PDDA films with and without external electrical field.

spectra were measured for the same conditions. So the results are comparable even though the difference in results (peak position, OD) are very small.

From these figures, it is clear that there are changes in absorption spectrum: peak position, optical density and wavelength at maximum absorption. They all increase with the number of bilayers, films made under an external field have lower absorption and peak wavelength than those of films without an applied external field. The electrical field influences the electronic states of the chromophores, induces excited state dipoles and results in a change in the dipole moment upon electronic excitation. There are permanent dipoles within the films. They can be aligned upon interaction with the field in one direction. These dipoles will be aligned with the field, causing a change in polarization and change the internal field. But in ground state (0 field, no excitation), permanent dipoles are randomly distributed, and the average orientation angle is 0. This give rise to the changes in optical absorption spectrum between two samples.

This measurement is implemented under 0 external field, so the shift of absorption peak from 0V field to 0.47 V is clearly due to the internal field deference of two samples. The ESA thin film technique possess the unique advantage that the molecular (chromophores) may be aligned by an external field, so the randomly distributed dipoles (that for no applied field tend to cancel each other, so the overall net field is zero) are now aligned in the same external field direction. An internal field is then created, and the observed spectrum shift is produced. Notice that the shifts are not apparent. This is due to weak external voltage applied to samples. Higher voltages should give rise to increased shifts. But in practice, higher voltage (higher than 0.6 volt) will cause damage to the electrodes (ITO film), so we can not apply very high voltage to samples to achieve greater shift. In this case, more sensitive measurement methods are desirable to detect the molecular or chromophores alignment in terms of average alignment angle. One of these techniques is the second harmonic generation (SHG) measurement. By employing this technique, the average tilt angle θ of molecular, chromophores and the dipoles in quantum dots away from the substrate normal is determined by [20]

$$\cos\theta = \left(\frac{\chi^{(2)}_{zzz}}{\chi^{(2)}_{zxx}} \right)^{\frac{1}{2}} , \qquad (2.15)$$

where $\chi^{(2)}_{zzz}$ and $\chi^{(2)}_{zxx}$ are second order susceptibility of films at different directions. They can be obtained by measuring the fundamental and second harmonic intensities of the P- and S- polarized states of light. This is a good method to measure the alignment angle,

but it is not available in our lab. So this measurement was not performed even though it is very useful.

It is interest to compare this result with poling experiments of spin coated electro-optic films implemented by Mortazavi [21]. In his experiment, spin coated electro-optic films were poled at elevated temperatures, and absorption was measured at different times before and after corona poling. It was found that the absorbance of unpoled films is lower than for poled films, that unpoled film has the highest absorbance, and that the absorption peak shifted to longer wavelength. Immediately after poling, absorbance was reduced to almost half of the highest absorbance, and the absorbance increased with time to approach the highest absorbance (unpoled films). After 10 days, no further increase in absorbance was noticed. The final absorbance reached 78% of the highest absorbance. This result is similar to results reported here, in that the role of the poling field in his experiment is the same as the applied external field in my film process. They all aid the alignment of dipoles in the films. On the other hand, it tells us that absorbance measurement can be helpful to investigate the dipole orientation.

Based on Boltzmann statistics, the distribution function is [22]

$$g(\theta) = \frac{\exp(-\Delta W / kT)}{\int_0^{\pi} \exp(-\Delta W / kT) \sin\theta d\theta} \quad , \tag{2.16}$$

where $\Delta W = \mu E$ is the total interaction energy between the molecule and electric field, μ is the dipole moment, E is electric field, θ is the angle between μ and E, and k is the Boltzmann constant. The order parameter, which describes the orientation of dipoles, is

$$\Phi = ½(3<\cos^2\theta>-1)\ , \tag{2.17}$$

where $<\cos^2\theta>$ can be determined by

$$\frac{A_{//}}{A_0} = 3 < \cos^2\theta >= 3L(\frac{\mu E_i}{kT}) \quad , \tag{2.18}$$

and

$$\frac{A_{\perp}}{A_0} = \frac{3}{2} < \sin^2\theta >= \frac{3}{2}[1 - L(\frac{\mu E_i}{kT})\ ] \quad , \tag{2.19}$$

where $A_{//}$ is the absorbance of a poled sample measured with the electric field polarized parallel to the poling direction, $A_{\perp}$ is the absorbance of a poled sample measured with the electric field polarized perpendicular to the poling direction, and A_0 is the absorbance of an unpoled sample. All of these quantities should be measured at maximum absorption weavlength. Finally, the order parameter can be determined in terms of absorbance as

$$\Phi = 1 - \frac{A_{\perp}}{A_0} \quad , \tag{2.20}$$

Since the order parameter decreases with ΔK increase of absobance $A_{\perp}$ this agrees with experimental and literature results. Thus, in the process of film fabrication by means of ESA, the presence of an external field helps the alignment of molecules or dipoles. This affects not only the absorption spectrum, but also the electro-optic and nonlinear optic properties of films. This will be discussed in detail in the next chapter.

2.5.4 Comparison and process control of film growth by ESA technique

In the ESA process, many factors affect film growth, such as electro-chemistry properties of the solutions (zeta potential, coulomb interaction of cation and anion solutions), pH value, and the concentration of the solutions. In my study, effects of solution type, and pH value of solution on film growth are investigated, the purpose is to make uniform, stable, and thick films.

For polymeric electro-optic ESA films, chromophor PS-119 may be selected as electro-optic polymers. It is dissolved in water as an anion solution, and two cation type polymers are typically used; one is PAH, the other is PDDA. Figures 2-20 to 2-23 are the optical absorption spectra and growth properties of two such polymer electro-optic ESA films. It can be seen that both PS-119/PDDA (75 bilayers) and PS-119/PAH (200 bilayers) films grow linearly because absorption increases linearly with number of bilayer. They have their absorption peaks around 477 nm, with a slight difference (±2 nm). This suggests that the anions (PDDA or PAH) only cause small shift of the absorption peak of PS-119, because PS-119 binds with PDDA or PAH by electrostatic attracting, not by chemical bonding. But PS-119/PDDA film yields a higher absorption per bilayer (0.0153 abs./ bilayer) than that of PS-119/PAH film (0.0074 abs./ bilayer) and also a higher thickness per bilayer (2 nm/bilayer) than that of PS-119/PAH film (1.3 nm/bilayer), because PS-119 has stronger binding with PDDA than with PAH. The absorption coefficient α is almost the same ($\alpha_{PS\text{-}119/PDDA} = 0.0076$/nm, $\alpha_{PS\text{-}119/PDDA} = 0.0074$/nm).

In comparison with pervious results shown in Figures 2-17, 2-18 and 2-19, in which films have greater thickness, the absorbance and optical density do not increase

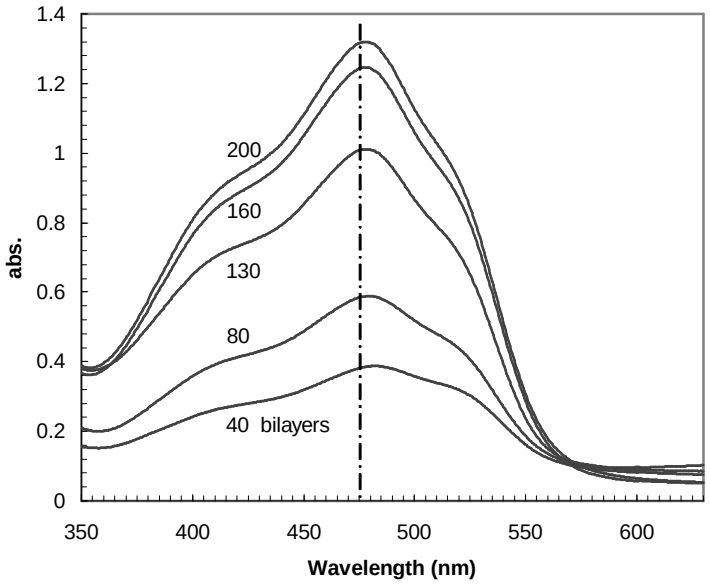

Fig. 2-20. Optical absorption spectra of PS-119/PAH films with different thicknesses (number of bilayers).

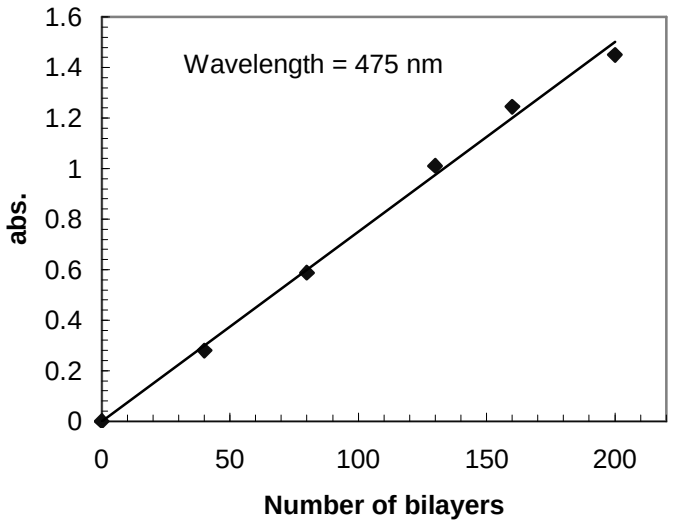

Fig. 2-21. Absorption varies with number of bilayers of PS-119/PAH films at peak position.

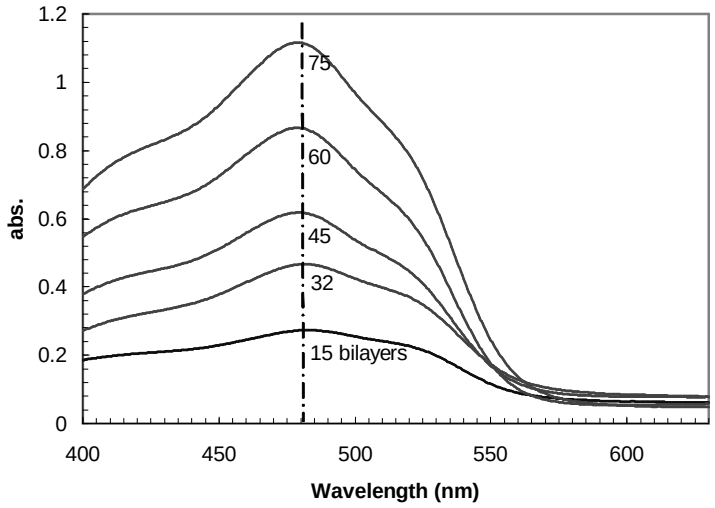

Fig. 2-22. Optical absorption spectra of PS-119/PDDA films with different thicknesses (number of bilayers).

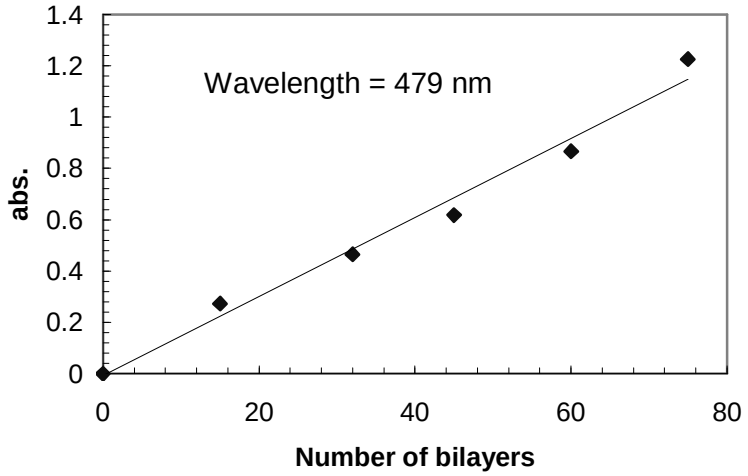

Fig. 2-23. Absorption varies with number of bilayers of PS-119/PDDA films at peak position.

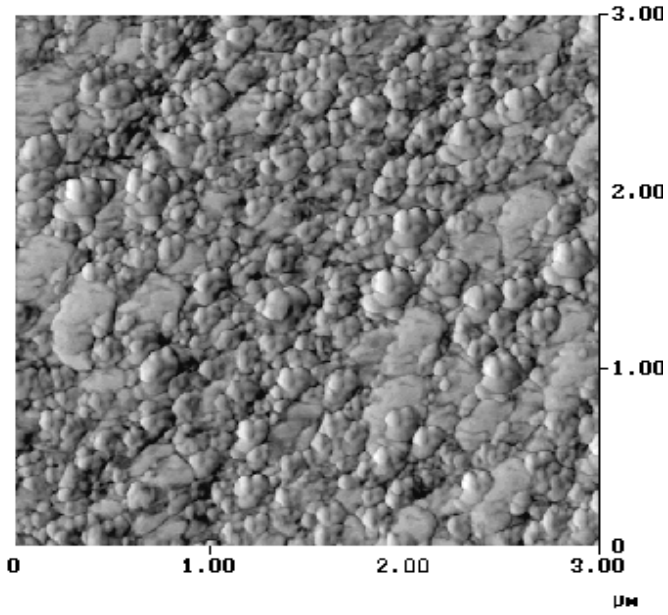

Fig. 2-24. AFM diagram of PS 119/PAH film, 200 bilayers.

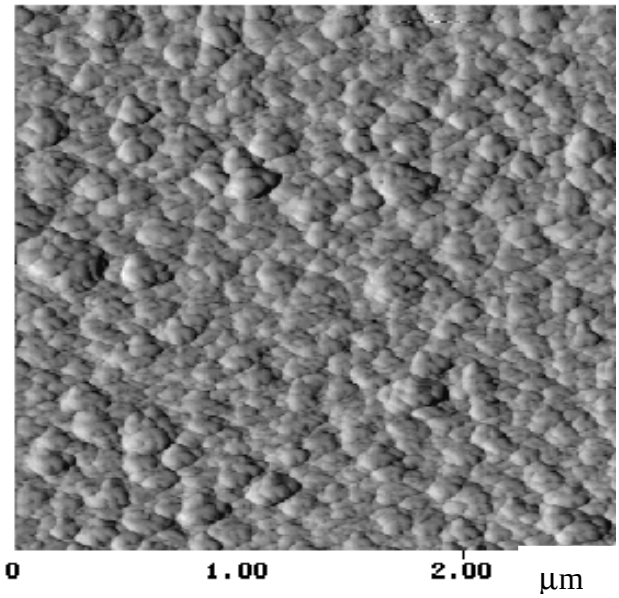

Fig. 2-25. AFM diagram of PS-119/PDDA film, 75 bilayers.

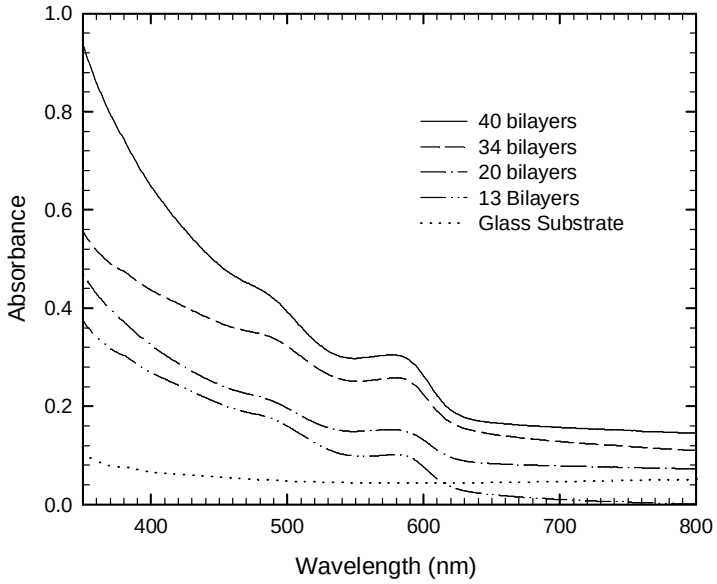

Fig. 2-26. Absorption spectrum verses number of bilayers, pH value of PDDA solution is 5.8.

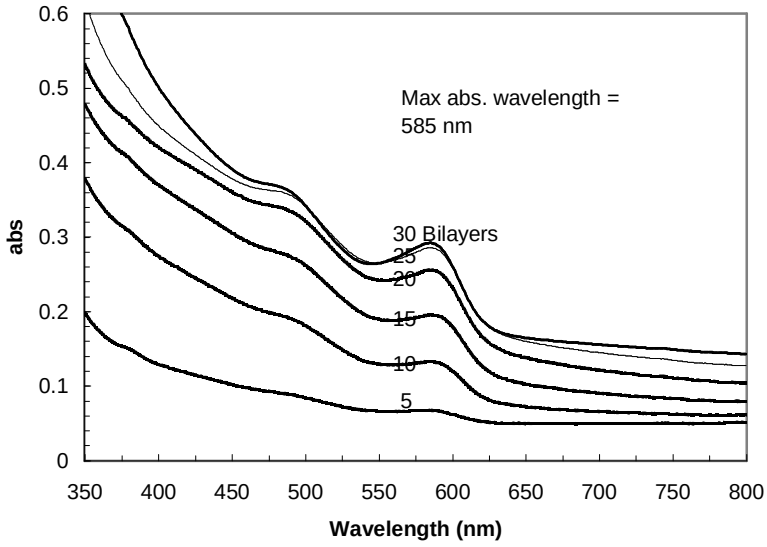

Fig. 2-27. Absorption spectrum verses number of bilayers, pH value of PDDA solution is 11.5.

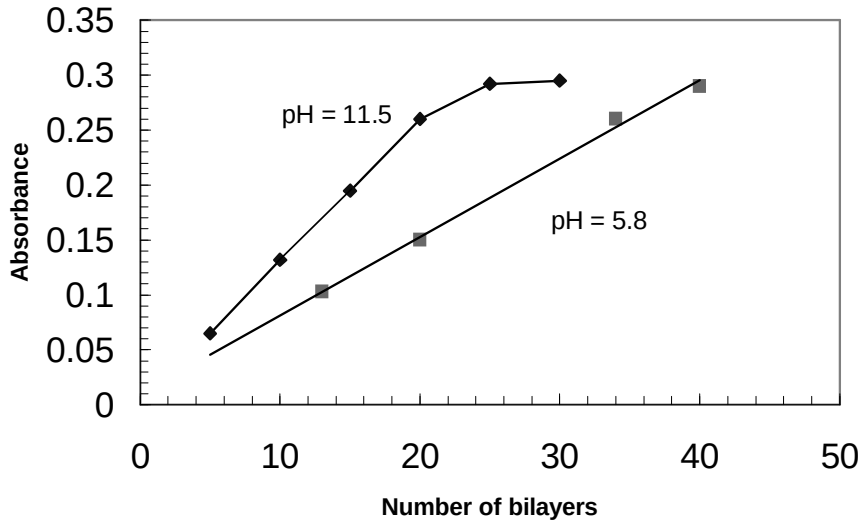

Fig. 2-28. Absorption varies with number of bilayers of CdSe/PDDA films at peak position (585 nm), pH value of PDDA solution is 5.8 and 11.5.

linearly with the number of bilayers if the number of bilayer is larger than 200. This means that for thicker films, film growth is not uniform, and absorbance and optical density per bilayer decreases with film thickness. This non-uniformity in film growth will also affect other film properties. This will be discussed in the follow chapter.

Figures 2-24 and 2-25 are AFM images of polymeric electro-optic films. From these pictures, there is no apparent morphological difference, and the film surfaces are uniform and dense, with no cracks, no pin holes and low roughness.

The pH value of the solution is also an important process parameter that affects film growth. In our experimental synthesis of nano-cluster / polymer films, the anion solution the same (PDDA), but pH value is different and the effect of solution pH on film growth has been investigated. Figures 2-26, 2-27 and 2-28 illustrate absorption spectrum and versus the number of bilayers at different pH values of the PDDA solution.

Absorbance increases with film thickness (or number of bilayers), and the peak positions are not shifted, but film growth is different. At high pH, each bilayer causes higher absorbance, but film growth is not uniform. Growth slows down as the number of bilayers increases. Finally absorbance saturates and thickness no longer increases. In order to make thicker films, a PDDA solution with a lower pH value was used. The result is the same as for the electro-optic polymeric films, which have been discussed previously. Film growth is uniform, absorbance increases almost linearly with number of bilayers, and no saturation is reached, but absorbance per bilayer is lower than that for the higher pH value case.

2.5.5 Stability of nano-cluster and polymeric electro-optic films

A: Thermal, temporal and photo-chemistry stability

Stability of electro-optic and other polymer materials is an important issue for their practical uses. Now many polymers have been synthesized with supreme properties. For example, some polymers demonstrate electro-optic coefficients 5 to 10 times higher than those of traditional inorganic electro-optic crystals, and they are inexpensive, and easy to integrate with existing microelectronic processes. But they degrade with time and temperature, and are susceptible to various light and other electromagnetic ray irradiation effects.

Much effort has been expended on this problem. For films made by the ESA process, thermal stability has been investigated by K. L. Cooper and Yanjiang Liu et al [10, 23]. In their experiments, samples were heated up to 150C for several hours, and SHG

signal intensities were measured right before and after heating. It was found that the SHG intensity reduced to 75% of its initial value as temperature was raised. But the SHG intensity remained extremely stable as the temperature was maintained at 150C, and the SHG intensity almost returned to its initial value as the temperature returned to room temperature, with only a 9% loss. It also was reported that film thickness was decreased upon heating, and that the contact angle of ESA films changed with temperature, but they too could almost be restored to their initial values after cooling, and also only with slight changes. Comparing those experimental results with spin coated film results, it is indicated that ESA films possess higher stability to maintain their structures. Their molecular orientation or dipole moment alignment are highly resist to thermal perturbations and are capable of restoring to their initial state, with only minor decay.

As for temporal stability, the UV-vis absorption of several ESA films at different times (as long as 12 months after fabrication) were evaluated with no detectable change in absorption spectra (intensity, peak position , and optical density) found. For spin coated polymer films, many researchers have indicated that after poling at certain temperature, the absorption and optical and electro-optic properties decayed rapidly with time. Only after several hours, apparent changes can be observed. After several months, most of their electro-optic response may be lost[21]. By comparison, ESA films are much more stable than spin coated polymer films. This is one of the most impressive features of ESA process. It opens a possibility to produce highly stable electro-optic and other optical polymer films.

B: Photochemistry stability

It is found that, through experimental observations, intense optical beams leads to the darkening of both polymer and nano-cluster films. The same phenomena was also observed by other researchers. The darkened samples give low but fast electro-optic response, and the decay time in photo luminescence is also much shorter. This is related to the recombination of surface and trap states, but the exact reasons are still not clear. So during the measurement process, in order to avoid the darkening problem, and obtain consistent results, the beam intensity cannot be too high. For electro-optic coefficient measurement, the laser power should be lower than 40 mW, and performed as quickly as possible.

C: Oxidation - XPS results for CdSe films

XPS measurement was utilized in the study of oxidation of nano-clusters and the concentration of nano-clusters in films. Figures 2-29, 2-30 and 2-31 are the XPS results. Concentration units used in these figures are atomic %. From these spectra, one can see that the concentrations of Cd and Se in ESA films are around 6.10 and 2-3.75, which change slightly with ESA process parameters (such as pH values of solutions). Note that not all the Se combines with Cd to form CdSe nano-clusters. Here only 56.58% of the Se is alloy (CdSe). The other 43.42% of the Se is oxidized. By simple calculations, the concentration of CdSe quantum dots in this sample is 2.14%, and some SeO_x ($x < 3$) is in film. The concentration is rather constant over the entire sample area.

From the XPS spectrum of CdSe films, it is seen that Se has two kinds of states: alloy (CdSe) and oxidized Se. Se has the tendency to bond with both Cd and O to form CdSe and SeO_2. Because only a small part of the CdSe clusters are covered by polymer ligands

such as TOPO, it is highly possible that upon exposure to air, oxygen atoms attach onto the CdSe surface sites. This is accompanied by the transfer of electrons from Se to O, leading to the formation of SeO or SeO_2. SeO or SeO_2 then increase with time. As the formed SeO or SeO_2 deabsorbs to the cluster surface, the fresh CdSe surface is exposed to oxygen, and more Se atoms are oxidized. From thermodynamics, there are several possible oxidization reactions. Each reaction corresponds to a different reaction activation energy (ΔH_{298}^{0}) given by

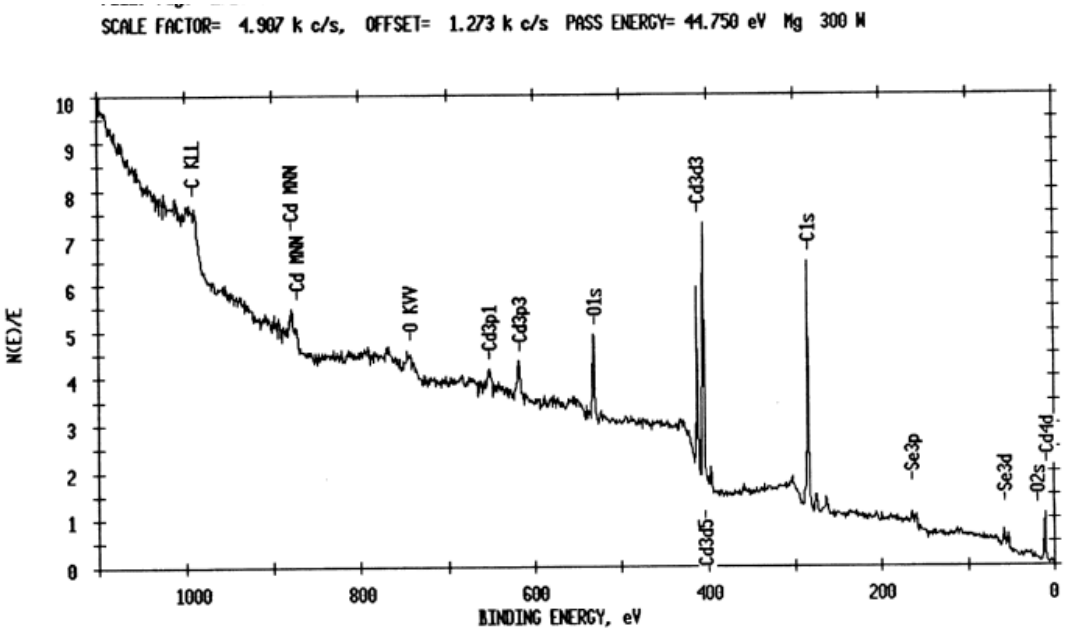

Fig. 2-29. XPS spectrum of CdSe-PDDA film made by ESA process, pH value of PDDA solution is11.5, concentrations are: Cd = 6.20, Se = 2.08 (atomic %).

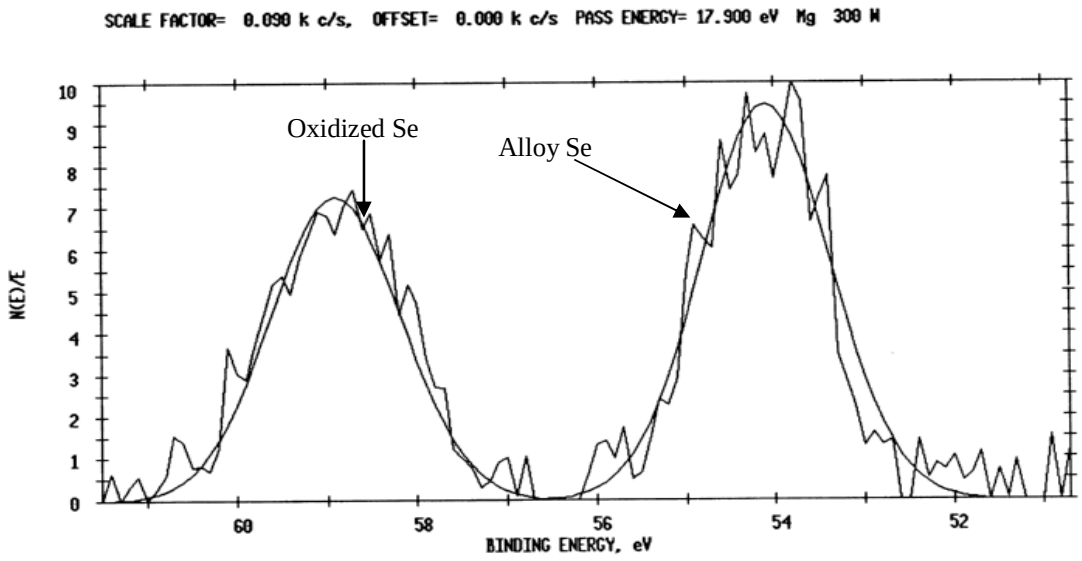

Fig. 2-30. XPS spectrum of CdSe-PDDA film made by ESA process, pH value of PDDA solution is11.5, concentrations are compound Se = 43.42, alloy Se = 56.58 (atomic %).

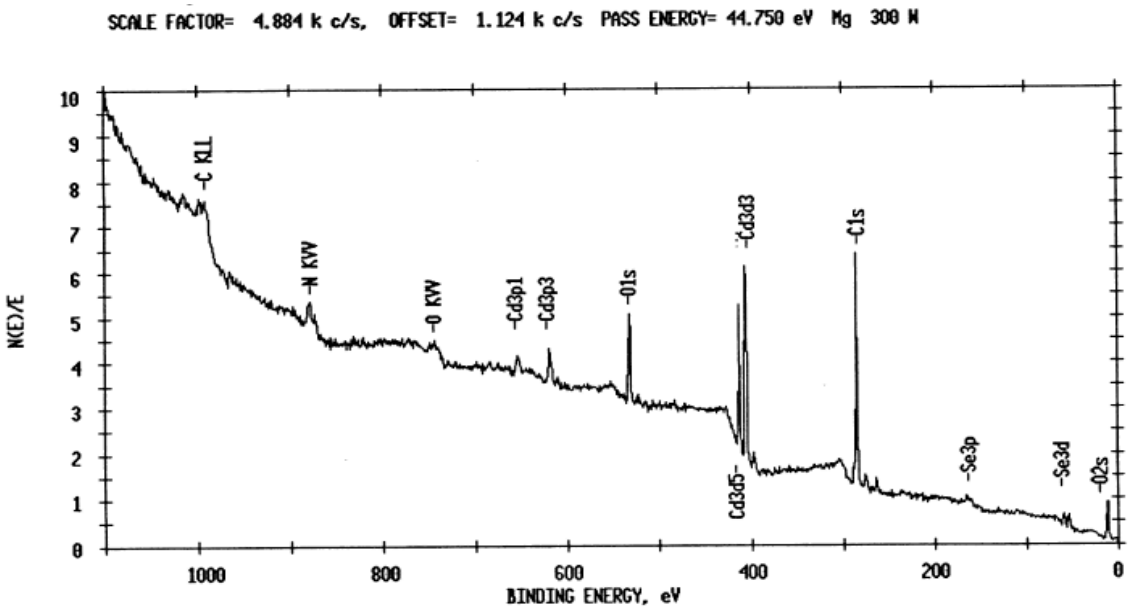

Fig. 2-31. XPS spectrum of CdSe-PDDA film made by ESA process, pH value of PDDA solution is5.8, concentration is Cd = 6.14, Se = 3.48 (atomic %).

The fourth reaction is most easy, so it is the most likely to occur, but in practice, most ligands are bonded to Cd, not to Se, so the yield of this reaction is low. Most of the reaction takes places according to the third process, and finally SeO_2 is formed.

Because of this reaction, in the process of film fabrication, the CdSe solution should be bubbled under a nitrogen atmosphere to prevent the clusters from oxidizing. Once oxidized, the surface double electrical layer at the cluster-solvent interface will be depleted, the zeta potential will reduce greatly, clusters will precipitate, and the solution will degrade with time and finally can no longer be used. As a result, thick films (over 100 bilayers) can not be produced.

2.6. Conclusions

II-VI semiconductor nano-clusters have been synthesized, with particle diameters ranging from 4 nm to several tens of nanometers. The diameter can be controlled by controlling reaction time and temperature, and particle size can be monitored easily by regular UV-vis abs. spectrum measurement during the synthesis process. In order to make high quality nano-clusters, the synthesis temperature should be higher then 300C. There is a difference in peak positions of absorption and photo luminescence spectra, related to defects in nano-crystals. Larger CdS particles have larger differences than small CdSe particles. Particle sizes measured by absorption spectrum and by HRTEM are very close. Based on quantum mechanical theory, shifts as a function of particlesize can be predicted, but the theoretical results are far from the experimental results.

By dispersing nano-clusters in a polymer host, two kinds of electro-optical films are fabricated. One is by the ESA process, another is by the spin coating process. ESA

films have much stronger absorption than spin coated films, and slight blue shift in peak position wavelength. Photo luminescence spectra also show a blue shift of ESA films with respect to spun films. One reason for this is an internal field induced shift, due to the different structure of these two films. Another reason is a particle size induced shift, due to atomic particle size selection in the ESA process. Larger and poorly capped particles are precipitated, so particles in ESA films are a little smaller than particles in spin coated films. Control of the pH value of the cationic solution is important, in that higher pH results in thicker film per bilayer, but resulting film growth is not uniform. Growth will slow down and finally saturate. At low pH, the film grows uniformly, but the thickness per bilayer is low.

Polymeric electro-optic films may be fabricated by the ESA technique. Effects of applying an external electrical field during the ESA process on film growth and properties have also been investigated. Peak position, optical density and wavelength at maximum absorption, all increase with number of bilayers, and films made under external fields have lower absorption and peak wavelength than those of films fabricated without an external field. These results are related to the order parameter, and indicate that molecule alignment can be improved by the application of an external field during the process of ESA film growth.

Stability of nano-cluster and polymeric electro-optic films was also investigated. XPS spectrum measurement was employed to detect to the composition. It was found that Se is partially oxidized, only 56% of the Se binds to Cd to form CdSe nano-clusters, and CdSe solution is not stable in air, so the synthesis reaction, solution preparation and ESA film growth process should be implemented under an N_2 atmosphere. The

thermodynamic mechanism and possible reactions are discussed. One of the most significant features of films made by ESA techniques is their supreme temperature and temporal stability, in comparison with spin coated films. However films are sensitive to various forms of irradiation, and intense beams lead to the darkening of both polymer and nano-cluster films, and as a result film properties are subject to change.

2.7. References

1. P. Horan, W. Blau, Phas. Tran., 24-26, 605(1990).
2. A. D. Yoffe, Adv. Phys., 42, 173(1993).
3. Lide Zhang, Jimei Mu: Nano-materials. LiaoNing Scientific Inc. (1994).
4. M. Jacobsohn and U. Banin, J. Phys. Chem. B, 104, 1(2000).
5. S. A. Blanton, R. L. Leheny, M. A. Guyot-Sionnest, Phys. Revi. Lett., 79, 865 (1997).
6. Mark Green, P. O'Brien, Chem. Comm., 2235 (1999).
7. M. G. Bawendi, Conf. Elec. Phot, Plenum Press, 339 (1995).
8. C. B. Murray, D. J. Norris, and M. G. Bawendi, J. Amer. Chem. Soc., 115, 8706 (1993).
9. Kriste M. Lenahan, Yanjing Liu, You-Xiong Wang, Richard O. Claus, SPIE, 3675 (1999).
10. K. L. Cooper: ESA of linear and nonlinear optical thin films. Ph. D dissertation, Virginia Tech, (1999).
11. R. M.Shaffert: Electrophotography. Wiley, New York, (1975).

12. M. Kuno, J. K.Lee, B. O. Dabbousi, F. V. Mikulec, and M. G. Bawendi, J. Chem. Phys, 106, 9869(1997).

13. R. Rossetti, J. L. Ellison, J. M. Gibson and L. E. Brus, J. Chem. Phys., 80, 4464 (1984).

14. R. A. Smith: Semiconductors. 2nd ed, Cambridge University Press, Lodon, (1979).

15. Z.Adam Peng and Xiaogang Peng, J. Amer. Chem. Soc., 123, 183 (2001).

16. Michael A. Olshavsky and Harry R. Allcock, Chem. Mate., 9,1367 (1997).

17. L. E. Brus, J. Chem. Phys., 80, 9(1984).

18. L. E. Brus, Appl. Phys. A, 53, 465 (1991).

19. V. L. Colvin and A. P. Alivisators, J. Chem. Phys., 97, 730(1992).

20. J. R. Heflin, C. Figura, and D. Marciu, Appl. Phys. Lett, 74, 495 (1999).

21. M. A. Mortazavi, A. Knoesen, and S. T. Kowel, J. Opti. Soc. Amer. B, 6, 733 (1989).

22. K. Yamaoka and E. Charney, J. Amer. Chem. Soc., 94, 8963 (1972).

23. C. Figura, D. Marciu, Y. Liu, Y. X. Wang, K. Lenahan, R. O. Claus and J. R. Heflin, Proc. Amer. Chem. Soc. (Boston), Aug., 1998.